



# Ion beam effects of 26.0 MeV $\text{Cu}^{7+}$ ions in thin metallic and insulating films during Heavy Ion ERDA measurements



H. Mavhungu<sup>a,d</sup>, M. Msimanga<sup>b,c,\*</sup>, T. Hlatshwayo<sup>d</sup>

<sup>a</sup> NECSA, Radiation Science Division, PLABS, P.O. Box 582, Pretoria 0001, South Africa

<sup>b</sup> Tshwane University of Technology, Department of Physics, P Bag X680, Pretoria 0001, South Africa

<sup>c</sup> iThemba LABS, National Research Foundation, P. Bag 11, WITS 2050, Johannesburg, South Africa

<sup>d</sup> University of Pretoria, Department of Physics, Private Bag X20 Hatfield, Pretoria 0028, South Africa

## ARTICLE INFO

### Article history:

Received 3 December 2014

Received in revised form 22 January 2015

Accepted 16 February 2015

Available online 28 February 2015

### Keywords:

Thin film

Heavy Ion ERDA

Ion beam damage

Electronic sputtering

Ion beam analysis

## ABSTRACT

We report on an investigation carried out to determine effects of the probing beam on the structure of typical metallic and insulating thin films during Elastic Recoil Detection Analysis (ERDA) using a heavy ion beam. Metallic niobium nitride (NbN) and insulating calcium fluoride ( $\text{CaF}_2$ ) thin films (used as test samples) were irradiated by 26.0 MeV  $^{63}\text{Cu}^{7+}$  ions to fluences of  $1.70 \times 10^{14}$  ions/cm<sup>2</sup> and  $2.70 \times 10^{14}$  ions/cm<sup>2</sup>, respectively. The effects of irradiation on the structural properties of the films were studied using Rutherford Backscattering Spectrometry (RBS), X-ray diffraction (XRD) and Atomic Force Microscopy (AFM). RBS results showed a significant (18%) reduction in the thickness of the  $\text{CaF}_2$  film due to electronic sputtering compared to only 1% reduction in the NbN film. XRD results showed no significant peak shifts in both films, but rather formation of unidentified peaks in the insulating film. AFM results indicated a substantial decrease in the average surface roughness of the insulating film and only a nominal increase in that of the metallic film. Results of electronic sputtering yield measurements carried out by ERDA are explained in terms of both the Coulomb explosion and the inelastic thermal spike models.

© 2015 Elsevier B.V. All rights reserved.

## 1. Introduction

Thin solid films are used in a wide range of applications in modern technology from decorative, optical and hard protective coatings through to high frequency filters, solar cells and wire sensors [1]. Transition metal nitride thin films for example are found in many applications due to a combination of refractory and metallic properties. Niobium nitride (NbN) for instance is used as a superconductor and in detectors for infrared light [2]. It has attracted much attention due to its interesting physical properties and the associated technological applications, next to those of titanium nitride [3]. As another example, thin film alkali-earth fluorides and multilayer structures that include such layers are known to be prospective materials for optics, photonics and chemical sensors. Calcium fluoride ( $\text{CaF}_2$ ) films in particular have been used for a long time in many optical components due to its exceptional transparency in the ultra violet (UV) as well as in the infra-red (IR) spectral domain [4].

Many advanced thin-film materials such as the examples cited above derive their functional properties from compounds

containing light elements. Nuclear analytical techniques have become indispensable in the development of thin film based technologies. Ion beam analysis (IBA) techniques that use ion beams from particle accelerators have a competitive advantage in that they can provide important information about the concentration, distribution and location of light elements in thin film matrices much more readily and directly than non-nuclear spectrometries [5].

Elastic Recoil Detection Analysis (ERDA) is an IBA technique based on the elastic forward recoiling of target atomic nuclei (generally) lighter than the projectile [6]. It is a complementary scattering technique to Rutherford Backscattering Spectrometry (RBS) and is particularly useful for easy depth profiling of hydrogen (H, D, and T) and helium isotopes in surfaces and thin films. The variant of ERDA using projectiles heavier than helium is known as Heavy Ion ERDA. When performed with  $\text{He}^+$  projectiles, ERDA is generally non-destructive, but as the incident ion beam particles become heavier, the effect of the beam on the surface layers of the target sample may become significant, depending on the beam energy and fluence, angle of incidence and nature of the target [7–9]. At MeV energies the dominant mode of beam-target energy exchange is electronic stopping (leading to electronic sputtering) [7]. Much of the work done on electronic sputtering in the grazing incidence ERDA configuration has focused on relatively high

\* Corresponding author at: Tshwane University of Technology, Department of Physics, P Bag X680, Pretoria 0001, South Africa.

E-mail address: [msimanga@tut.ac.za](mailto:msimanga@tut.ac.za) (M. Msimanga).

energy ( $>1.0$  MeV/u) incident ions [10–13]. At lower energies ( $0.1 \leq E \leq 0.5$  MeV/u), apart from work by Gordillo et al. [14], not much else has been reported. This latter energy region is where most small accelerator labs involved in heavy ion Time-of-Flight (ToF) ERDA operate [9,15–20]. The Heavy Ion ERDA technique at iThemba LABS Gauteng [19] was set up recently and there are continual studies to optimise its performance subject to existing infrastructural limitations. This study investigates the effects of the probing beam on the structure (i.e. thickness, crystallinity and roughness) of typical metallic and insulating thin films during ERD analysis using 26.0 MeV  $^{63}\text{Cu}^{7+}$  ion beams.

## 2. Experimental

Thin films of NbN/Si were grown by reactive magnetron sputtering of a NbN target. The target was sputtered by  $\text{Ar}^+$  ions for 15 min at 100 W RF power. Pre-cleaned silicon substrates were placed 50 mm above the target for film deposition. The base pressure of the system was below  $7.2 \times 10^{-1}$  mbar during the sputtering process.  $\text{CaF}_2/\text{Si}$  samples were prepared by electron beam evaporation of granular  $\text{CaF}_2$  onto silicon substrate pieces. The base pressure in the evaporation chamber was maintained below  $10^{-7}$  mbar during deposition. Both film types were characterised for thickness, crystallinity and surface roughness before and after Heavy Ion ERD irradiation analysis.

Irradiation of the films was carried out in the ERDA configuration using the 6 MV Tandem accelerator at iThemba LABS Gauteng. The NbN/Si and  $\text{CaF}_2/\text{Si}$  thin films were each irradiated by a beam of 26.0 MeV  $^{63}\text{Cu}^{7+}$  ions at average beam currents of 13 nA and 16 nA, respectively, corresponding to ion rates of  $1.2 \times 10^{10} \text{ s}^{-1}$  and  $1.4 \times 10^{10} \text{ s}^{-1}$ . The projectile beam hit the target samples at a grazing incidence angle of  $15^\circ$  to the sample surface. The ToF-energy detector telescope used for the detection and identification of recoil ions is set at a forward scattering angle of  $30^\circ$  to the initial beam direction [19]. The beam fluence  $\Phi$  was calculated from the irradiation time ( $t$ ), beam current ( $I$ ), and the beam spot area ( $A$ ) on the target:

$$\Phi = \frac{It}{qeA}, \quad (1)$$

where  $q$  is the ionic charge (7) and  $e$  is the electron charge ( $1.602 \times 10^{-19} \text{ C}$ ).

Pressure in the target chamber during Heavy Ion ERDA measurements was in the order of  $10^{-7}$  mbar. The metallic film was irradiated to a fluence of  $1.70 \times 10^{14} \text{ ions/cm}^2$  and the insulating film was irradiated to  $2.70 \times 10^{14} \text{ ions/cm}^2$ . Structural characterisation of both films was carried out before and after Cu irradiation to ascertain the effect of the probing beam on the films. Rutherford Backscattering (RBS) measurements were carried out at the University of Pretoria's 2 MV Van De Graff accelerator using 1.6 MeV  $\text{He}^+$  ions to measure (any) variation in the thickness and composition of the films. The analysing particle beam was collimated to a spot of 1 mm diameter. A ring-shaped electrode in front of the target was kept at a negative potential of 200 V to suppress secondary electrons. Sufficient counting statistics was obtained by collecting an integrated charge of 8  $\mu\text{C}$ . Backscattered particles were measured at  $165^\circ$  by a surface barrier detector telescope with an acceptance angle of  $2^\circ$ . XRD analyses were performed using a Bruker D8 Advance™ diffractometer to determine possible beam effects on the structure of the films. The diffractometer was operated at a voltage of 40 kV and a current of 40 mA, generating 8 keV  $\text{K}_\alpha$  X-rays from a copper target. AFM analyses were carried out using the Dimension Icon® Atomic Force Microscope from Bruker™ to measure the surface roughness and morphology of the films.

## 3. Results and discussion

### 3.1. Film thickness measurement results

RBS energy spectra of the metallic NbN and the insulating  $\text{CaF}_2$  films obtained before and after irradiation are shown in Figs. 1a and 1b, where the horizontal axis represents backscattered beam energy (in channel numbers). The SIMNRA simulation code [21] was used to obtain the thickness and stoichiometry of the films. However, the simulation plots are not included in Figs. 1a and 1b to avoid obscuring the comparison between the pristine and irradiated films. Both films were found to be stoichiometric, before and after irradiation. The arrows in both figures indicate the surface energy positions of the different atomic species detected in the films. In Fig. 1a, what appears as a nitrogen surface peak is readily fitted by assuming presence of a native  $\text{SiO}_2$  layer on the Si substrate. The thickness of the sandwiched oxide layer was estimated to be about  $150 \times 10^{15} \text{ at/cm}^2$ . Iron contamination, possibly a residual impurity in the RF sputtering chamber, was detected in the NbN film. The uncertainty in the measured thickness values is a convolution several contributions. The main contributor is the uncertainty in the SRIM stopping force for He ions traversing the films – 3.5% [22]. Other (minor) factors include the RBS detector energy resolution (quoted at 20 keV at 5.46 MeV), 0.5% in the beam energy spread and 0.21% uncertainty in the SIMNRA code [23]. All these factors add up to an effective 3.6% uncertainty in the film thickness.

The thickness values obtained from the SIMNRA simulations are summarised in Table 1. There was a small, rather insignificant ( $<1\%$ ) decrease in the thickness of the metallic film after irradiation, while a significant (18%) reduction in thickness was observed in the insulating film. Similar behaviour in other types of insulating films has also been observed by other workers [7–9].

### 3.2. Phase identification analysis

For phase identification XRD data analysis was done with the proprietary Bruker EVA™ search and match software. The identified phases in the NbN and  $\text{CaF}_2$  films are displayed in Figs. 2a and 2b. The XRD spectrum of the metallic film before ion irradiation shows Bragg reflections at  $2\theta$  equal to  $35^\circ$ ,  $39^\circ$ ,  $58^\circ$  and  $71^\circ$  corresponding respectively to (111), (200), (220) and (311) reflections of the NbN face centered phase. After irradiation the Bragg reflections are at the same  $2\theta$  values indicating no peak shift

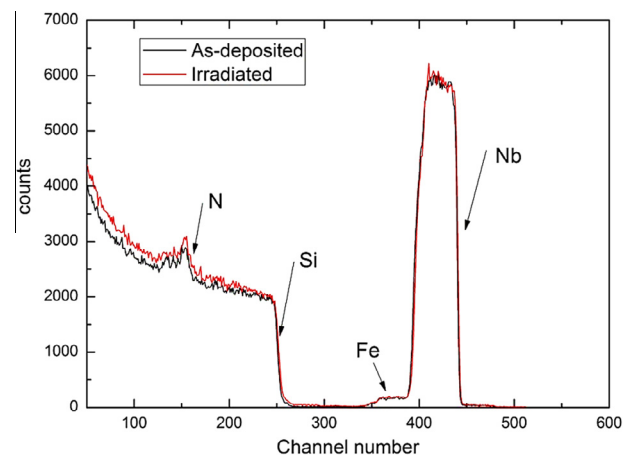


**Fig. 1a.** RBS spectrum of the as-deposited (black) and Cu-irradiated (red) NbN/Si layer. (For interpretation of the references to colour in this figure legend, the reader is referred to the web version of this article.)

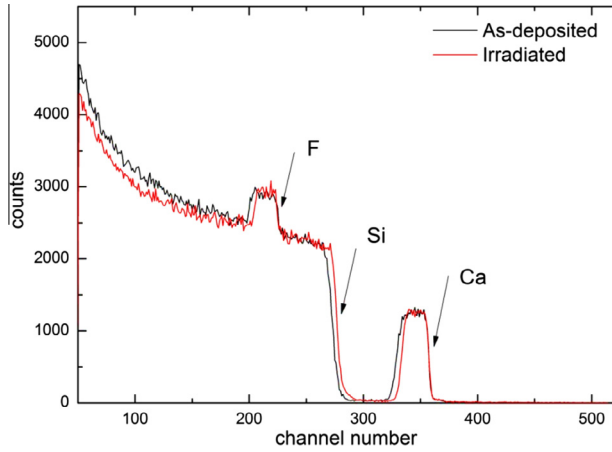


**Fig. 1b.** RBS spectrum of the as-deposited (black) and Cu-irradiated (red)  $\text{CaF}_2/\text{Si}$  layer. (For interpretation of the references to colour in this figure legend, the reader is referred to the web version of this article.)

**Table 1**

Measured thickness values of metallic (NbN/Si) and insulating ( $\text{CaF}_2/\text{Si}$ ) films before and after 26.0 MeV  $\text{Cu}^{7+}$  ion irradiation.

Target film	Film thickness ( $10^{15}$ atoms/ $\text{cm}^2$ )		
	Before irradiation	After irradiation	% decrease
NbN	1005	995	0.99
$\text{CaF}_2$	952	781	18

due to the  $^{63}\text{Cu}^{7+}$  ion beam. For the insulating  $\text{CaF}_2$  film, before irradiation, Bragg reflections show up at  $2\theta$  equal to  $28^\circ$ ,  $47^\circ$  and  $57^\circ$  corresponding respectively to (111), (220) and (311) crystal planes. After ion irradiation the initial Bragg reflection  $2\theta$  angles are again unchanged, but now a broad unidentified peak appears centered around  $58^\circ$ . This new peak is thought to be composed of a number of several peaks overlapping due to formation of unknown phases caused by ion beam induced mixing between the film and the substrate. Scherrer's equation [24] was used to obtain a qualitative check of the effect of irradiation on the crystallite size  $L$ :

$$L = k\lambda / \beta \cos \theta \quad (2)$$

where  $k$  is the polarization factor,  $\lambda$  is the wavelength of the  $\text{Cu}_{K\alpha}$  line (1.5406 Å),  $\beta$  is the full width at half maximum (FWHM) and  $\theta$  is the Bragg angle. Not much change is observed in crystallite sizes of both films along any of the peak domains. The crystallite size of the NbN film along the [111] domain for example, changes only slightly from 5.6 nm to 5.8 nm after ion irradiation. This is an insignificant change though, given the  $0.005^\circ$  uncertainty in the Bragg angle and about 4% error in  $\beta$ . For the  $\text{CaF}_2$  film the crystallite size remains unchanged at 8.9 nm along the same domain. The lattice spacing of crystal planes was also calculated using Bragg's Law equation and was found to be unchanged in both film types after irradiation.

### 3.3. Surface topography

The surface topography of both films was analysed by AFM before and after ion irradiation. Typical scan images are shown in Figs. 3 and 4 for the metallic and insulating films, respectively. Initial average roughness values were measured to be 0.28 nm for the NbN film and 5.4 nm for the  $\text{CaF}_2$  film. The NbN film images in Fig. 3 suggest a nominal change in average surface roughness after irradiation. The measured change was an increase from 0.28 nm to

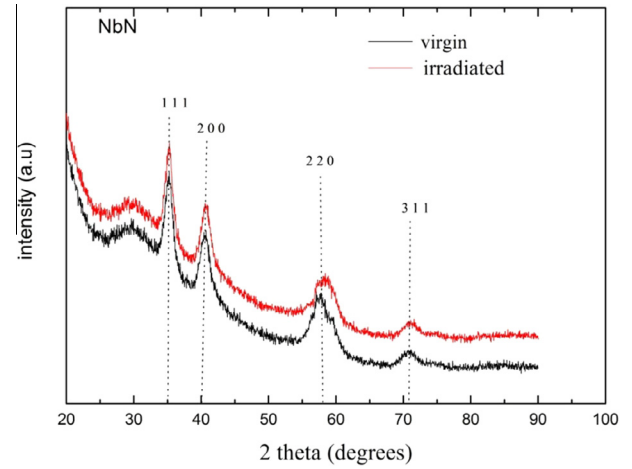


**Fig. 2a.** XRD spectra of as-deposited (black) and irradiated (red) NbN/Si with the vertical dotted lines indicating diffraction peak positions. (For interpretation of the references to colour in this figure legend, the reader is referred to the web version of this article.)

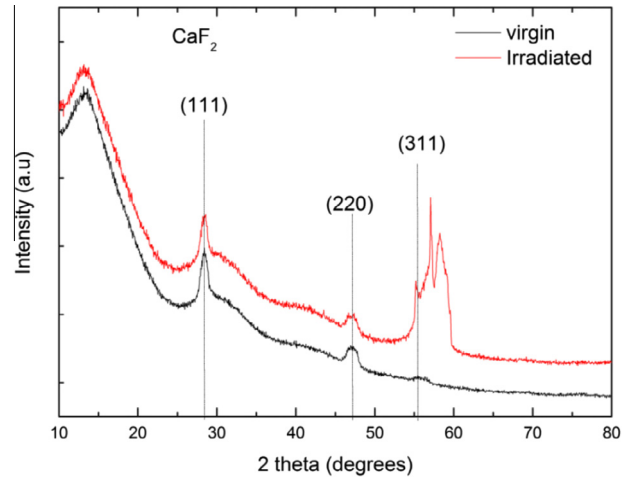


**Fig. 2b.** XRD spectra of as deposited (black) and irradiated (red)  $\text{CaF}_2$  with the vertical dotted lines indicating diffraction peak positions. (For interpretation of the references to colour in this figure legend, the reader is referred to the web version of this article.)

0.30 nm. The waviness observed in the irradiated film could be due to a mismatch between the thermal expansion coefficients of the NbN film and the native  $\text{SiO}_2$  layer between the deposited film and the Si substrate. The average surface roughness of the insulating film decreased significantly after irradiation, smoothening from 5.4 nm down to 2.3 nm. The topography of a solid thin film during ion irradiation is determined by the interplay between surface roughening that occurs due to sputtering and smoothening that is induced by material transport during surface diffusion [25]. It appears that for the metallic film, the sputtering process, though materially insignificant according to the thickness measurement results, was more predominant than atomic surface diffusion hence the apparent increase in surface roughness. Fig. 4 suggests an agglomeration of the  $\text{CaF}_2$  surface hillocks after irradiation. This could be due to beam induced localised melting of the pristine film during irradiation, followed by immediate recrystallization thereafter. The end result then is that the average height of surface undulations decreases slightly due to lateral intermixing and coalescence of the hillocks into larger and smoother clusters, which in turn results in the observed decrease in surface roughness [26].

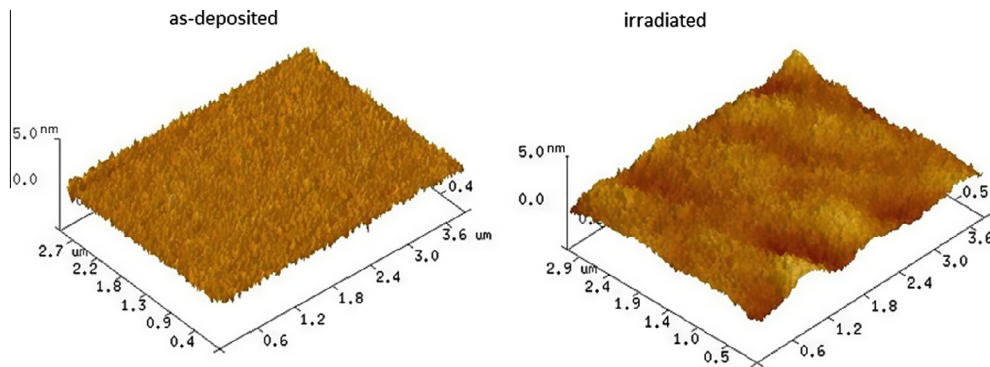


Fig. 3. AFM images of pristine and irradiated NbN films.

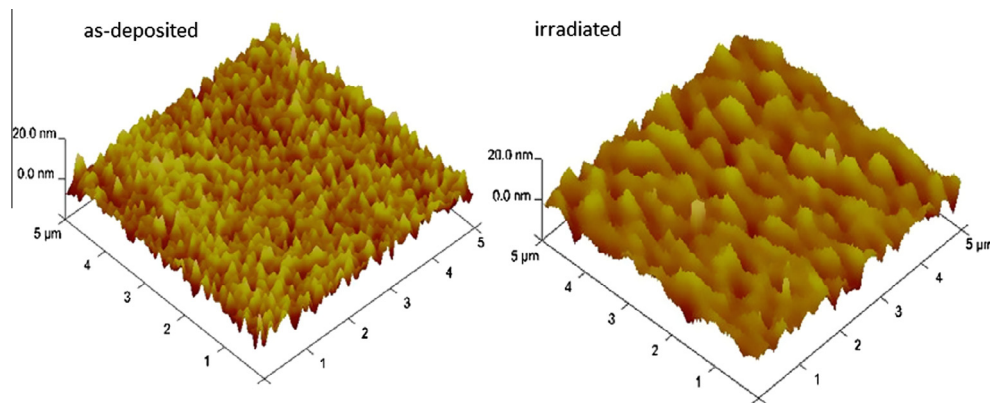


Fig. 4. AFM images of pristine and irradiated CaF<sub>2</sub> films.

### 3.4. Electronic sputtering yield

The beam fluences of the order of  $10^{14}$  ions/cm<sup>2</sup> delivered to the two target films described above are typical fluences that most target films would receive during ERD analysis at iThemba LABS, and possibly at any other ion beam analysis laboratory. Further measurements were carried out to measure film thickness as a function of beam fluence. A different pair of both film types was irradiated to even higher (than usual ERD analysis) fluences. The metallic film was irradiated to a fluence of up to  $3.8 \times 10^{14}$  ions/cm<sup>2</sup> and the insulating film irradiated up to  $4.8 \times 10^{14}$  ions/cm<sup>2</sup>. The event-by-event mode data acquisition system used at iThemba LABS for Heavy Ion ERD analyses facilitates offline replay of data in selected time slots. In this way it is possible to monitor and measure the thickness variation of a film over time, which directly translates to thickness variation with beam fluence. Fig. 5 shows the variation in relative atomic concentration of the two films with beam fluence, in units of areal density.

The result shown in Fig. 5a indicates that electronic sputtering of the NbN film was insignificant, in agreement with the RBS result obtained earlier. The thickness of the film was largely unchanged even up to the highest fluence and the stoichiometry of the film remains the same. On the other hand, as shown in Fig. 5b, there was considerable sputtering of the insulating CaF<sub>2</sub> film. The areal density of both Ca and F atomic species is seen to decrease with fluence. For this set of experimental conditions the sputtering rate of calcium atoms by 26.0 MeV <sup>63</sup>Cu<sup>7+</sup> ions was measured to be 38 atoms/ion and that of fluorine atoms 176 atoms/ion.

According to SRIM [22] calculations, the stopping force (*S*) of 26.0 MeV Cu ions in both NbN and CaF<sub>2</sub> is dominated by electronic

stopping (the ratio  $S_{\text{nuclear}}/S_{\text{electronic}}$  is 0.81% for NbN and 0.76% for CaF<sub>2</sub>). It is therefore expected that the energy transfer between the projectile ion and the target atoms is mainly due to electronic stopping of the incident ion. In the electronic sputtering regime, two seemingly competing physical models that attempt to describe electronic sputtering are currently accepted; the Coulomb explosion [27] and the inelastic thermal spike models [28]. The idea central to both mechanisms though, is that rupture of material along the ion track leads to molecular motion and eventual sputtering at the surface/vacuum interface.

Bringa and Johnson argue that the two models describe two successive stages of the same phenomenon [29]. According to the Coulomb explosion model, the transiting projectile ion creates a highly charged region along its path due to electronic excitation and creation of excitons in insulators. Coulomb repulsion in this region leads to atomic expulsion before relaxation takes place i.e. within  $\sim 10^{-16}$ – $10^{-14}$  s of projectile energy deposition [10]. Energy is then transferred to lattice atoms via electron–phonon coupling only at a later stage,  $10^{-14}$ – $10^{-11}$  s after the initial interaction. According to Bringa and Johnson, sputtering of atoms further occurs from a heated cylindrical region due to a thermal spike induced evaporation process. This latter stage is what is described by the inelastic thermal spike model.

Bringa and Johnson's argument can be used to explain the different sputtering yields observed in our two film types. The energy deposited in the metallic NbN film is quickly dissipated throughout the lattice structure before any sufficient built-up of a high charge density region, due to high mobility of the electron cloud. The subsequent electron–phonon coupling is too weak to create a thermal pressure wave or thermal spike sufficient to lead to any significant



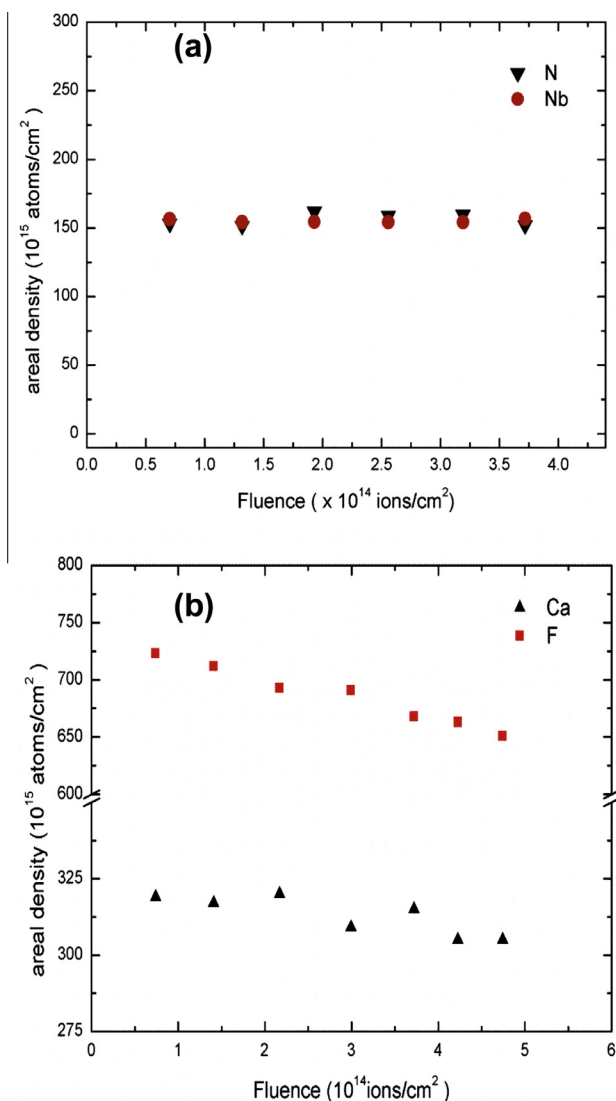


Fig. 5. Areal atomic density of (a) niobium nitride and (b) calcium fluoride thin films during ERD analysis with 26.0 MeV  $^{63}\text{Cu}^{7+}$  ions.

evaporation. In the insulating  $\text{CaF}_2$  however, ionisation and exciton creation is localised enough along the projectile path to create a high charge density region to an extent that Coulombic expulsion can take place. Subsequent energy transfer is in the form of thermal energy to the lattice through relaxation of excited states. And because of the dense localisation, this transfer is in the form of a high pressure wave or a 'thermal spike', leading to atomic evaporation. The challenge with this explanation is to determine how much of the measured sputtering yield is due to Coulomb explosion and how much of it is due to the inelastic thermal spike effect. In the end, however, if not for fundamental reasons, the distinction may be immaterial for ion beam analysis applications. What is needed though is more experimental data to facilitate reliable modelling and prediction of the electronic sputtering process to the same degree of accuracy and reliability as collisional sputtering. There is a general need for systematic investigations of the relationship between beam type, energy and sputter yield of various materials to get a consolidated view of electronic sputtering phenomena for applications in MeV ion beam techniques such as Heavy Ion ERDA and MeV Secondary Ion Mass Spectrometry (SIMS).

#### 4. Conclusion

Thin films of NbN and  $\text{CaF}_2$  on silicon substrates were irradiated by 26.0 MeV  $\text{Cu}^{7+}$  ions in the ERDA configuration. Structural characterisation results indicate more pronounced beam effects in the insulating film compared to the metallic one; effects which can be attributed to greater localisation of the deposited incident beam energy in the insulating film compared to the conducting one. The surface roughness of the  $\text{CaF}_2$  film decreased by over 50% (as opposed to a  $\sim 7\%$  increase in that of the NbN film), and the thickness also decreased quite substantially. The roughness of a film has a direct effect on the depth resolution of a measurement in ion beam analysis, more so in Heavy Ion ERDA [30]. It affects the accuracy of depth profiles where, on the one hand broadening of profile edges due to film roughness could be misinterpreted as layer intermixing, and on the other, smoothening of a surface layer could also lead to artificially sharp interlayer boundaries. This highlights the need for determining film roughness before and after ERD analysis of insulating films and incorporating any changes in the data analysis.

The sputtering results presented in this work also reinforce literature findings that electronic sputtering by swift heavy ion irradiation is much more prevalent in insulators than in conductors. While the results are important for furthering understanding of fundamental ion beam-matter interactions, there are immediate practical implications for Heavy Ion ERD analysis of insulating films. Corrections have to be made to measured film thicknesses to account for ion beam induced thickness reduction. Unfortunately the corrections can only be reliable if the sputtering rate is known or can be predicted accurately, which points to the need for more experimental data to aid in the development of accurate theoretical models.

#### Acknowledgements

The authors gratefully acknowledge NECSA, Tshwane University of Technology, University of Pretoria and iThemba LABS Gauteng for financial support and experimental facilities. We would also like to thank Drs. D. Wamwangi and M. Nkosi for sample preparation.

#### References

- [1] L. Kolakieva, R. Kakanakov, Nanostructured materials, thin films and hard coatings for advanced applications, in: 2nd International Conference on Nanostructured Materials, Thin Films and Hard Coatings for Advanced Applications, Sozopol, Bulgaria, May 24–27, 2009, Trans Tech Publications Inc., 2010.
- [2] S. Chaudhuri, M.R. Nevala, T. Hakkarainen, T. Niemi, I.J. Maasilta, Infrared pulsed laser deposition of niobium nitride thin films, *IEEE Trans. Appl. Supercond.* 21 (3) (2011).
- [3] W. Lengauer, Transition metal carbides, nitrides and carbonitrides, in: R. Riedel (Ed.), *Handbook of Ceramic Hard Materials*, Wiley-VCH, Verlag GmbH, 2000, p. 202.
- [4] N. Emre Çertin et al., The structural, optical and morphological properties of  $\text{CaF}_2$  thin films by using Thermionic Vacuum Arc (TVA), *Mater. Lett.* 91 (2013) 175–178.
- [5] N. Dytlewski, Improvement of the reliability and accuracy of nuclear analytical techniques, IAEA Coordinated Research Project Proposal F11013 (2007).
- [6] J. Tirira, Y. Serruys, P. Trocellier, *Forward Recoil Spectrometry: Applications to Hydrogen Determination in Solids*, Plenum Press, New York, 1995.
- [7] W. Assmann, M. Toulemonde, C. Trautmann, Electronic sputtering with swift heavy ions, *Top. Appl. Phys.* 110 (2007) 401–450.
- [8] S. Gosh et al., Structural effect on electronic sputtering of hydrogenated amorphous carbon films, *Solid State Commun.* 120 (2001) 445–450.
- [9] J. Jensen, D. Martin, A. Surpi, T. Kubart, ERD analysis and modification of  $\text{TiO}_2$  thin films with heavy ions, *Nucl. Instr. Meth. B* 268 (2010) 1893–1898.
- [10] M. Toulemonde, W. Assmann, C. Trautmann, F. Gruner, H.D. Mieskes, H. Kucal, Z.G. Wang, Electronic sputtering of metals and insulators by swift heavy ions, *Nucl. Instr. Meth. B* 212 (2003) 346–357.
- [11] S. Ghosh, D.K. Avasthi, A. Tripathi, D. Kabiraj, S. Singh, D.S. Misra, Electronic sputtering of carbon allotropes, *Nucl. Instr. Meth. B* 219–220 (2004) 973–979.

- [12] M. Kumar, S.A. Khan, F. Singh, A. Tripathi, D.K. Avasthi, A.C. Pandey, Influence of grain size on electronic sputtering of LiF thin films, *Nucl. Instr. Meth. B* 256 (2007) 328–332.
- [13] R.K. Pandey, M. Kumar, S.A. Khan, T. Kumar, A. Tripathi, D.K. Avasthi, A.C. Pandey, Study of electronic sputtering of CaF<sub>2</sub> thin films, *Appl. Surf. Sci.* 289 (2014) 77–80.
- [14] N. Gordillo, R. Gonzalez-Arrabal, A. Rivera, F. Munnik, F. Agulló-López, Stopping power dependence of nitrogen sputtering yields in copper nitride films under swift-ion irradiation: exciton model approach, *Nucl. Instr. Meth. B* 289 (2012) 74–78.
- [15] J.K. Kim et al., A TOF spectrometer for elastic recoil detection, *Nucl. Instr. Meth. B* 140 (1998) 380–388.
- [16] A. Razpet, P. Pelicon, Z. Rupnik, M. Budnar, Development of a time-of-flight telescope for ERDA at the Jožef Stefan Institute, *Nucl. Instr. Meth. B* 201 (2003) 535–542.
- [17] A. Harjunmaa, T. Sajavaara, K. Arstila, K. Kukli, J. Keinonen, Thin film nanolaminate analysis by simultaneous heavy ion recoil and X-ray spectrometry, *Nucl. Instr. Meth. B* 219–220 (2004) 773–777.
- [18] S. Giangrandi, T. Sajavaara, B. Brijis, K. Arstila, A. Vantomme, W. Vandervorst, Low-energy heavy-ion TOF-ERDA setup for quantitative depth profiling of thin films, *Nucl. Instr. Meth. B* 266 (2008) 5144–5150.
- [19] M. Msimanga, D. Wamwangi, C.M. Comrie, C.A. Pineda-Vargas, M. Nkosi, T. Hlatshwayo, The new Heavy Ion ERDA set up at iThemba LABS Gauteng: multilayer thin film depth profiling using direct calculation and Monte Carlo simulation codes, *Nucl. Instr. Meth. B* 296 (2013) 54–60.
- [20] Y. Zhang et al., New ion beam materials laboratory for materials modification and irradiation effects research, *Nucl. Instr. Meth. B* 338 (2014) 19–30.
- [21] M. Mayer, SIMNRA User Guide, Report IPP 9/113, Max-Planck-Institut für Plasmaphysik, Garching, Germany, 1997.
- [22] J.F. Ziegler, M.D. Ziegler, J.P. Biersack, SRIM – The stopping and range of ions in matter (2010), *Nucl. Instr. Meth. B* 268 (2010) 1818.
- [23] N.P. Barradas, K. Arstila, G. Battistig, M. Bianconi, N. Dytlewski, C. Jeynes, E. Kótai, G. Lulli, M. Mayer, E. Rauhala, E. Szilágyi, M. Thompson, International Atomic Energy Agency intercomparison of ion beam analysis software, *Nucl. Instr. Meth. B* 262 (2007) 281.
- [24] A. Patterson, The Scherrer formula for X-ray particle size determination, *Phys. Rev.* 56 (10) (1939) 978–982.
- [25] S. Thomas, H. Thomas, D.K. Avasthi, A. Tripathi, R.V. Ramanujan, M.R. Anantharaman, Swift heavy ion induced surface modification for tailoring coercivity in Fe–Ni based amorphous thin films, *J. Appl. Phys.* 105 (2009) 033910.
- [26] N. Pahwa, A.D. Yadav, S.K. Dubey, A.P. Patel, A. Singh, D.C. Kothari, Structure and surface analysis of SHI irradiated thin films of cadmium telluride, *J. Nano Electron. Phys.* 4 (3) (2012) 03003.
- [27] R.L. Fleischer, P.B. Price, R.M. Walker, *Nuclear Tracks in Solids: Principles and Applications*, University of California Press, Berkeley, 1975.
- [28] M. Toulemonde, Ch. Dufour, A. Meftah, E. Paumier, Transient thermal processes in heavy ion irradiation of crystalline inorganic insulators, *Nucl. Instr. Meth. B* 166–167 (2000) 903–912.
- [29] E.M. Bringa, R.E. Johnson, Coulomb explosion and thermal spikes, *Phys. Rev. Lett.* 88 (2002) 165501.
- [30] T. Sajavaara, K. Arstila, A. Laakso, J. Keinonen, Effects of surface roughness on results in elastic recoil detection measurements, *Nucl. Instr. Meth. B* 161–163 (2000) 235–239.